Available online at www.sciencedirect.com
SCIENCE DIRECT®
Earth and Planetary Science Letters 248 (2006) 263–275
EPSL
www.elsevier.com/locate/epsl

Oxygen isotopic disequilibrium in plagioclase–corundum–hercynite xenoliths from the Voisey's Bay Intrusion, Labrador, Canada

J. Mariga [a], E.M. Ripley [a,*], C. Li [a], K.D. McKeegan [b], A. Schmidt [b], M. Groove [b]

[a] Department of Geological Sciences, Indiana University, Bloomington, IN 47405, USA
[b] Department of Earth and Space Science, University of California, Los Angeles, CA 90095-1567, USA

Received 16 December 2005; received in revised form 22 May 2006; accepted 24 May 2006
Available online 3 July 2006
Editor: R.W. Carlson

Abstract

Xenoliths of metamorphic country rocks are locally abundant within breccia sequences in gabbroic to troctolitic rocks of the Voisey's Bay Intrusion, Labrador, Canada. Thermochemical interaction with mafic magma has produced restite assemblages in the xenoliths that are composed of Ca-rich plagioclase, corundum, hercynite and minor magnetite. Hercynite was produced as a result of the breakdown of garnet and pyroxene that were originally present in the metamorphic rocks, as well as by the replacement of corundum, which was itself a product of feldspar degradation during xenolith–magma interaction. Hercynite that replaces pyroxene and garnet is granular to bulbous, whereas that which replaces corundum is acicular to skeletal. Ion microprobe analyses indicate that oxygen isotopic equilibrium was neither established during retrograde cooling of the xenolith assemblage, nor during the replacement processes which led to both types of pseudomorphous hercynite. $\delta^{18}O$ values of hercynite that replaces garnet and pyroxene range from 5 to 11.5‰, and in part reflect the elevated $\delta^{18}O$ values of the protolith minerals. Hercynite that replaces acicular corundum is characterized by $\delta^{18}O$ values between 2.5 and 7.6‰. Oxygen isotopic equilibration with mantle-derived magma having a $\delta^{18}O$ value of ~5.5‰ should have produced values of hercynite near 2.5‰. Values of Δ (plagioclase–corundum) range between 0.2 and 6.1‰, whereas D (hercynite–corundum) values, which are expected to be near 0, may be as large as 9.6‰ at the sub-millimeter scale. Oxygen isotopic disequilibrium may have resulted in the xenoliths due to rapid withdrawal of partial melt, and to the crystallization of plagioclase and biotite bands around the xenoliths which prevented isotopic communication of xenoliths with enclosing mafic magma. Although diffusive transport of oxygen in the xenoliths should have been a viable mechanism for isotopic exchange, the lack of isotopic equilibration during cooling and the preservation of steep isotopic gradients in composite hercynite–corundum grains suggest that reaction and crystallization were necessary to promote oxygen isotopic exchange among minerals in the xenoliths contained within the Voisey's Bay Intrusion.

Keywords: xenoliths; mafic magma; oxygen isotopes; disequilibrium

1. Introduction

The Voisey's Bay Intrusion of Labrador, Canada, hosts Ni–Cu–Co sulfide mineralization that is closely associated with country rock xenoliths. Progressive reaction of the xenoliths with mafic magma produced a characteristic mineral assemblage consisting of

* Corresponding author. Tel.: +1 812 855 1196; fax: +1 812 855 7961.
E-mail address: ripley@indiana.edu (E.M. Ripley).

0012-821X/$ - see front matter © 2006 Elsevier B.V. All rights reserved.
doi:10.1016/j.epsl.2006.05.031

hercynite, Ca-rich plagioclase, corundum and minor magnetite [1]. Temperatures of contact metamorphism estimated from mineral equilibria are in the range of 700 to 900 °C [2–4]. It can be readily shown that the relatively small xenoliths (2–10 cm in diameter) in the Voisey's Bay Intrusion should have reached thermal equilibrium with ~1150 °C olivine–plagioclase bearing magma within days. Previous oxygen isotopic studies of bulk mineral separates from the xenoliths [2] indicate that despite the attainment of thermal equilibrium, oxygen isotopic equilibrium was not achieved. However, analyses of bulk mineral separates do not permit a spatial evaluation of $\delta^{18}O$ variations which may shed light on the mechanism of isotopic exchange during high-temperature melt–rock interaction, which remains poorly understood. In the Voisey's Bay Intrusion hercynite exhibits three distinct morphologies that are interpreted as representing pseudomorphic replacement of corundum, garnet, and hypersthene. Hercynite and corundum may be present as part of the same grain, and for this reason ion microprobe analyses of these minerals were undertaken to investigate the nature of oxygen isotopic fractionation accompanying the replacement process. The ion microprobe analyses were combined with analyses of garnet, plagioclase and pyroxene mineral separates to better constrain the isotopic effects associated with the formation of pseudomorphic hercynite in the Voisey's Bay Intrusion.

2. Geological setting of the Voisey's Bay deposit

The Voisey's Bay Ni–Cu–Co sulfide deposit is located in northern Labrador, Canada, approximately 30 km southwest of the Town of Nain (Fig. 1). The geology of the Nain area has been described by several authors [3–10], therefore, only a brief summary of regional and local geology is presented here. The Voisey's Bay deposit occurs along the suture of two distinct, approximately north–south trending, lithotectonic units called the Nain and the Churchill Provinces (Fig. 1). The collision of the two provinces took place during the 1.86–1.82 Ga Torngat orogeny. The Voisey's Bay deposit is hosted by a troctolitic intrusion that belongs to the Nain Plutonic Suite. The Nain Plutonic Suite consists of granite, anorthosite, and troctolitic intrusions that formed at 1.35 to 1.30 Ga [11,12].

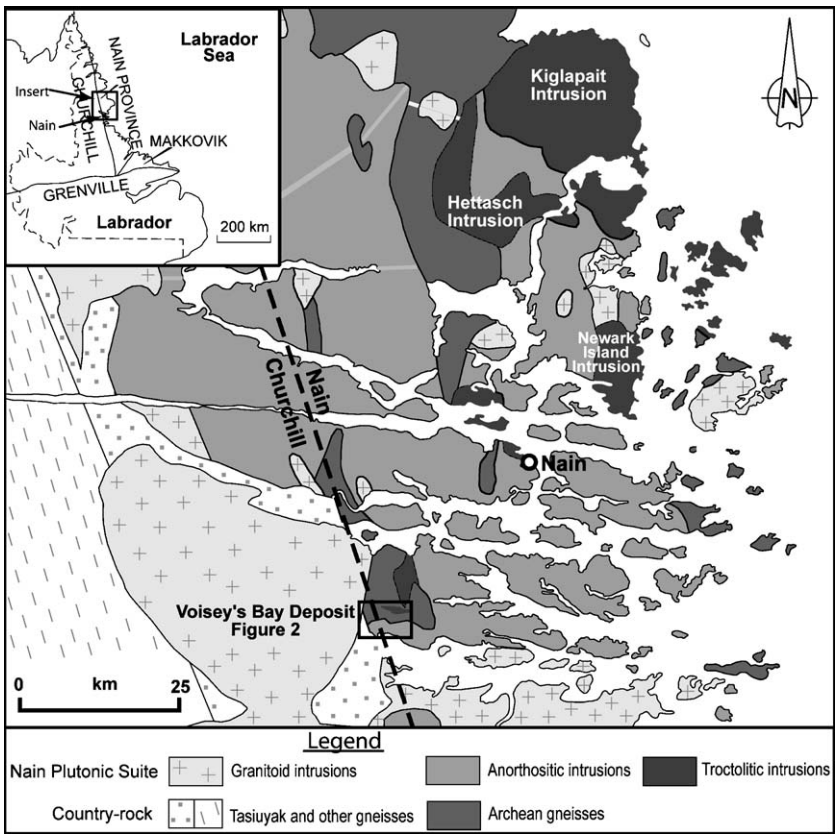

Fig. 1. Regional geology of the area around the Voisey's Bay deposit, (adapted from Ryan et al. [9]).

The Voisey's Bay Intrusion consists of two subchambers, the Reid Brook to the west and the Eastern Deeps to the east, and a feeder dike connecting them (see supplemental Fig. 1). Immediate country rocks to the intrusion include both metasedimentary and metaigneous rock types. The Paleoproterozoic Tasiuyak Gneiss occurs in the western portion of the area, and consists of garnet–sillimanite bearing, locally sulfidic and graphitic, quartzofeldspathic metasedimentary rocks. Metamorphosed intermediate to mafic igneous rocks, some of which are enderbitic, as well as quartzofeldspathic rocks, occur in the eastern portion of the area (supplemental Fig. 1). These rocks vary in age from Proterozoic to Archean. Small (2–10 cm) inclusions of country rocks are found in what is known as the Basal Breccia Sequence and the Feeder Breccia of the Voisey's Bay Intrusion. The Basal Breccia Sequence is a xenolith-bearing troctolitic to gabbroic unit that occurs near the base of the Eastern Deeps subchamber. The Feeder Breccia is a general term that refers to xenolith-bearing units in the conduit or dike. Variable percentages of Cu–Ni sulfides are found in the igneous matrix to the xenoliths; the interaction of mafic magma and country rocks is thought to be an important ingredient for magmatic sulfide ore formation [13]. The volume percentage of xenoliths in the breccia sequences varies from 5 to 50%.

3. Xenolith petrography

Details of the petrography, texture and characterization of the different types of xenoliths in the Voisey's Bay Intrusion have been given by [1]. In brief [1] distinguished five types of xenoliths that occur in the Voisey's Bay Intrusion: light-cored, dark-cored, laminated, massive, and variegated. All xenoliths in the Voisey's Bay Intrusion consist of hercynite, plagioclase, minor magnetite and in some cases corundum. The five types of xenoliths at Voisey's Bay record variations in the proportions and distribution of these minerals. In general the xenoliths contain about 30–70% hercynite, 0–40% corundum, and 20–40% anorthitic plagioclase. Magnetite constitutes not more than 10% of any xenolith. Massive xenoliths are characterized by concentrations of hercynite up to 70%. Hercynite, plagioclase and biotite define concentric bands around most xenoliths.

Three distinct morphologies of hercynite are observed in the xenoliths. The first type of hercynite is acicular and resembles the morphology of corundum. Acicular hercynite forms composite grains with corundum in light-cored and variegated xenoliths (supplemental Fig. 2). Corundum is mainly acicular or skeletal and can be present in the center of light-cored xenoliths as well as in some variegated xenoliths.

The second type of hercynite is granular in nature and is concentrated towards the rims of the xenoliths (supplemental Fig. 3a and b). This type of texture is also observed in granular pyroxene from the contact aureole.

The third type of hercynite is bulbous and exhibits a texture similar to that of garnet in the contact aureole of the Tasiuyak Gneiss. Bulbous hercynite is usually closely associated with magnetite and occurs mainly in the center of the xenoliths, surrounded by granular and/or vermicular textured hercynite (supplemental Fig. 3c and d). Vermicular and bulbous hercynite define a texture that mimics cordierite–orthopyroxene symplectites that are observed in the Tasiuyak Gneiss within the contact aureole of the Voisey's Bay Intrusion.

Table 1
$\delta^{18}O$ values of corundum from ion microprobe analysis

Drill core	Depth (m)	Zone	$\delta^{18}O$ (‰ VSMOW)
VB492	1005	S. Eastern Deeps	2.9
VB492	1005	S. Eastern Deeps	3.1
VB492	1005	S. Eastern Deeps	4.2
VB492	1005	S. Eastern Deeps	3.3
VB492	1005	S. Eastern Deeps	3.4
VB492	1005	S. Eastern Deeps	3.5
VB492	1005	S. Eastern Deeps	4.3
VB492	1005	S. Eastern Deeps	4.7
VB510	566.2	Eastern Deeps	1.9
VB510	566.2	Eastern Deeps	2.6
VB510	566.2	Eastern Deeps	2.8
VB510	566.2	Eastern Deeps	3.7
VB522	582.5	Discovery Hill	4.6
VB522	582.5	Discovery Hill	4.7
VB522	582.5	Discovery Hill	4.9
VB522	582.5	Discovery Hill	5.2
VB522	582.5	Discovery Hill	5.4
VB522	582.5	Discovery Hill	5.8
VB523	762	Eastern Deeps	3.6
VB523	762	Eastern Deeps	4.6
VB523	762	Eastern Deeps	4.8
VB523	762	Eastern Deeps	4.9
VB523	762	Eastern Deeps	5.1
VB523	762	Eastern Deeps	5.2
VB523	762	Eastern Deeps	5.2
VB523	762	Eastern Deeps	4.2
VB523	762	Eastern Deeps	5.4
VB523	762	Eastern Deeps	4.4
VB523	762	Eastern Deeps	5.5
VB523	762	Eastern Deeps	5.8
VB523	762	Eastern Deeps	5.9
VB523	762	Eastern Deeps	6.0
VB523	762	Eastern Deeps	6.1

4. Sampling and analytical methods

Samples used for this study were collected from drill cores in the Voisey's Bay Intrusion. Petrographic examination was performed using standard transmitted and reflected light microscopy.

Oxygen isotopic compositions of corundum and hercynite were obtained in situ using the UCLA CAMECA IMS 1270 ion microprobe. Parts of thin sections that exhibited the desired textures were cut and mounted, together with standards, onto a 2.5 cm diameter epoxy mount, which was gold coated before analysis. The mount was transferred into a sample chamber under ultra-high vacuum (10^{-9} Torr) aided by cryogenic trapping with liquid N_2 and bombarded with a mass-filtered $^{133}Cs^+$ beam (20 keV total impact energy). The $^{133}Cs^+$ beam was projected onto a 100 μm aperture, which resulted in ~3 nA beam and then focused onto the sample surface into ~20×30 μm spot. Surficial charge build-up was neutralized via a normal incidence electron gun and

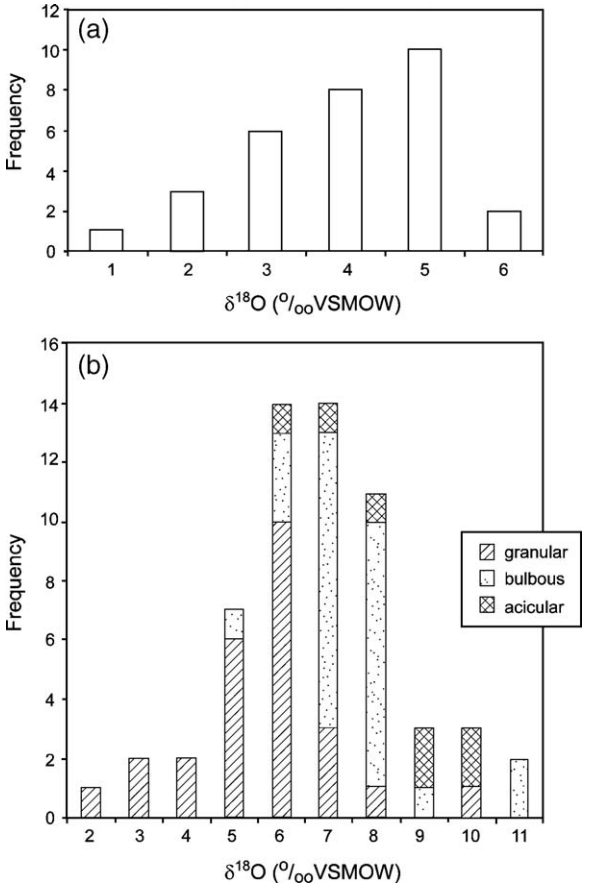

Fig. 2. (a) Histogram of $\delta^{18}O$ values of corundum from ion microprobe analyses. (b) Histogram showing the distribution of $\delta^{18}O$ values of acicular, bulbous and granular hercynites.

Table 2
$\delta^{18}O$ values of hercynite from ion microprobe analysis

Drill core	Depth (m)	Zone	Morphology	$\delta^{18}O$ (‰ VSMOW)
VB510	566.2	Eastern Deeps	Acicular	2.5
VB492	1005	S. Eastern Deeps	Acicular	3.3
VB510	566.2	Eastern Deeps	Acicular	3.9
VB492	1005	S. Eastern Deeps	Acicular	4.2
VB510	566.2	Eastern Deeps	Acicular	4.9
VB487	647	Reid Brook	Acicular	5.4
VB487	647	Reid Brook	Acicular	5.6
VB523	762	Eastern Deeps	Acicular	5.7
VB487	647	Reid Brook	Acicular	5.9
VB510	566.2	Eastern Deeps	Acicular	5.9
VB523	762	Eastern Deeps	Acicular	5.9
VB510	566.2	Eastern Deeps	Acicular	6.0
VB523	762	Eastern Deeps	Acicular	6.0
VB487	647	Reid Brook	Acicular	6.1
VB510	566.2	Eastern Deeps	Acicular	6.2
VB523	762	Eastern Deeps	Acicular	6.2
VB487	647	Reid Brook	Acicular	6.3
VB487	647	Reid Brook	Acicular	6.3
VB522	582.5	Discovery Hill	Acicular	6.4
VB522	582.5	Discovery Hill	Acicular	6.5
VB522	582.5	Discovery Hill	Acicular	6.5
VB487	647	Reid Brook	Acicular	7.4
VB523	762	Eastern Deeps	Acicular	7.6
VB510	566.2	Eastern Deeps	Acicular	7.8
VB510	566.2	Eastern Deeps	Acicular	8.9
VB492	1005	S. Eastern Deeps	Bulbous	5.0
VB487	647	Reid Brook	Bulbous	6.0
VB492	1005	S. Eastern Deeps	Bulbous	6.5
VB492	1005	S. Eastern Deeps	Bulbous	6.8
VB492	1005	S. Eastern Deeps	Bulbous	7.0
VB510	566.2	Eastern Deeps	Bulbous	7.4
VB510	566.2	Eastern Deeps	Bulbous	7.4
VB487	647	Reid Brook	Bulbous	7.5
VB510	566.2	Eastern Deeps	Bulbous	7.5
VB523	762	Eastern Deeps	Bulbous	7.5
VB492	1005	S. Eastern Deeps	Bulbous	7.6
VB510	566.2	Eastern Deeps	Bulbous	7.6
VB523	762	Eastern Deeps	Bulbous	7.8
VB487	316	Reid brook	Bulbous	7.9
VB487	316	Reid brook	Bulbous	8.0
VB510	566.2	Eastern Deeps	Bulbous	8.1
VB487	316	Reid brook	Bulbous	8.3
VB487	316	Reid brook	Bulbous	8.4
VB487	316	Reid brook	Bulbous	8.4
VB487	316	Reid brook	Bulbous	8.5
VB487	316	Reid brook	Bulbous	8.8
VB487	316	Reid brook	Bulbous	8.9
VB487	316	Reid brook	Bulbous	8.9
VB487	316	Reid brook	Bulbous	9.0
VB510	566.2	Eastern Deeps	Bulbous	11.5
VB523	762	Eastern Deeps	Bulbous	11.5
VB522	582.5	Discovery Hill	Granular	6.7
VB523	762	Eastern Deeps	Granular	7.0
VB522	582.5	Discovery Hill	Granular	8.6
VB522	582.5	Discovery Hill	Granular	9.1
VB523	762	Eastern Deeps	Granular	9.7
VB510	566.2	Eastern Deeps	Granular	10.2
VB523	762	Eastern Deeps	Granular	10.4

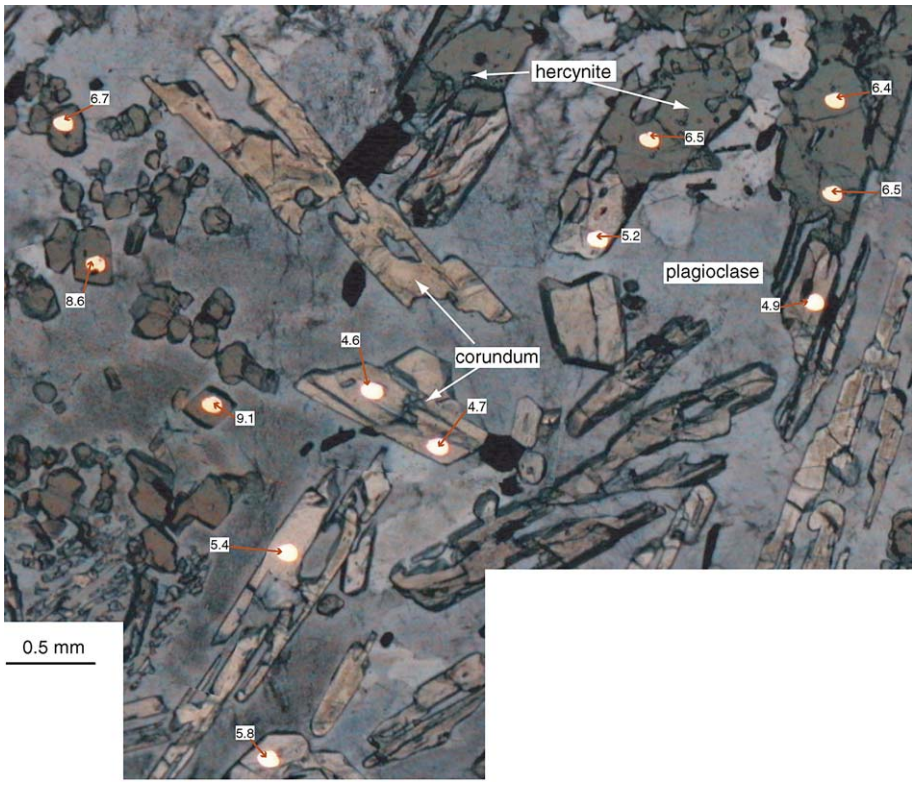

Fig. 3. Photomicrograph showing ion microprobe sites and distribution of $\delta^{18}O$ values in sample VB522–582.5 from the Discovery Hill section of the Viosey's Bay Intrusion. All $\delta^{18}O$ values are in per mil relative to VSMOW.

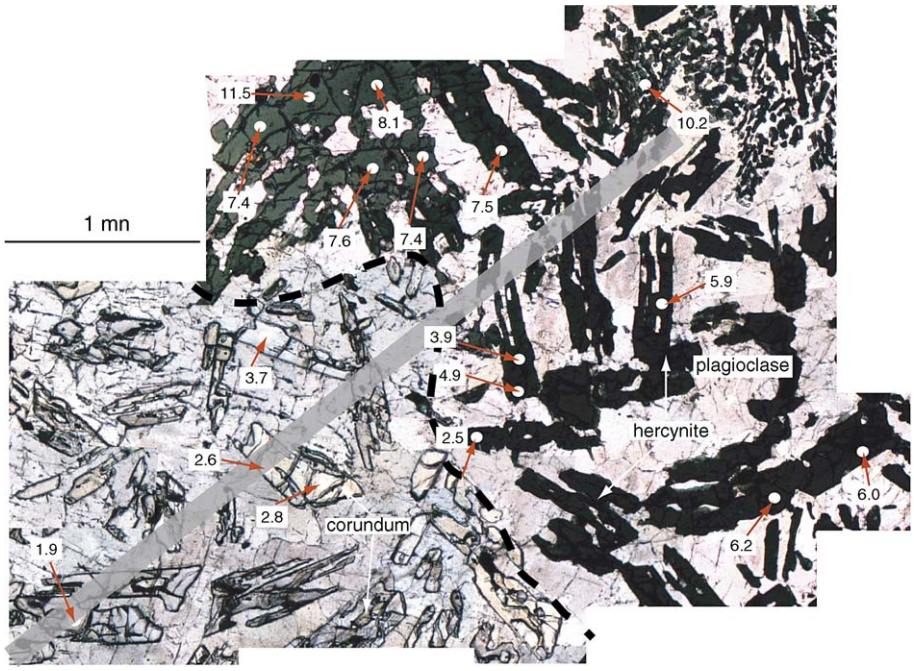

Fig. 4. Photomicrograph showing ion microprobe sites and distribution of $\delta^{18}O$ values in sample VB510–566.0 from the Eastern Deeps zone of the Viosey's Bay Intrusion. All $\delta^{18}O$ values are in per mil relative to VSMOW. The shaded line from the lower left to the upper right is the traverse line shown in Fig. 7.

negative secondary ions were accelerated at 10 keV. The energy bandpass for secondary ions was 50 eV and the mass spectrometer was tuned to a mass resolving power of 2000. Following a 3 min presputter period, $^{16}O^-$ and $^{18}O^-$ ions were simultaneously detected in two Faraday (FC) detectors with count rates on the order of $\sim 1.5\times10^9$ cps (3×10^6 cps). Integration time was 100 s, resulting in typical in-run precision of ~0.1‰. Raw intensities were corrected for detector baseline variations which were intermittently monitored by measuring FC background with the primary ion beam blanked. Areas that were close to grain boundaries, cracks and impurities were avoided.

Thirty-three corundum and 62 hercynite measurements were undertaken over three measurement sessions. To determine instrumental mass fractionation, a total of 13 laser ruby and 37 spinel (USNM 163728) analyses were performed at the beginning and intermittently throughout the analytical sessions. Prior to ion microprobe analysis at UCLA, fragments of these standards were analyzed at the Indiana University Stable Isotope Research Facility using a Finnigan MAT 252 stable isotope ratio mass spectrometer following conventional BrF_5 fluorination methods [14]. Analyses of NBS-28 quartz in this laboratory yield a value of 9.6±0.2‰ (VSMOW). Analytical uncertainties of individual isotopic measurements on the laser ruby and spinel samples were ~0.05‰, and sample reproducibility (external precision) was±0.2‰. Oxygen yields for spinel were 98 to 100%, whereas those for laser ruby were between 90 and 95%. The laser ruby and spinel 163728 are characterized by $\delta^{18}O$ values of 15.7 and 5.9‰, respectively. Russell et al. [15] previously reported a laser fluorination value for spinel 163728 of 4.95±0.1‰. The reason for this ~1‰ discrepancy is not resolved, but because the uncertainty for the standard directly influences the accuracy of the ion microprobe results, a systematic bias of the hercynite $\delta^{18}O$ values is possible. Another source for instrumental fractionation in ion microprobe oxygen isotope analysis arises from compositional differences in standards and unknowns known as matrix effects. While FeO contents of Voisey Bay hercynite (24–26 wt.%) are higher than those of spinel 163728 (19 wt.%; Russell et al. [15]), the maximum documented matrix effect in spinel between 0 and ~20 wt.% is ~0.5‰ [15] and therefore of second order relevance. Matrix effects are also likely to be insignificant for corundum which has pure end-member compositions in both standards and unknowns. Moreover, bulk mineral separates of corundum and hercynite yielded conventional values between 2.0 and 6.8‰, and 2.9 and 10.7‰, respectively [2], which agree closely with the ranges obtained by ion microprobe spot analyses. The average value of corundum determined by conventional and ion microprobe analyses is also similar (~5‰). This provides an independent check for the adequacy of instrumental mass fractionation corrections of the ion microprobe data. Because hercynite $\delta^{18}O$ values vary with grain morphology (see below), an overall average

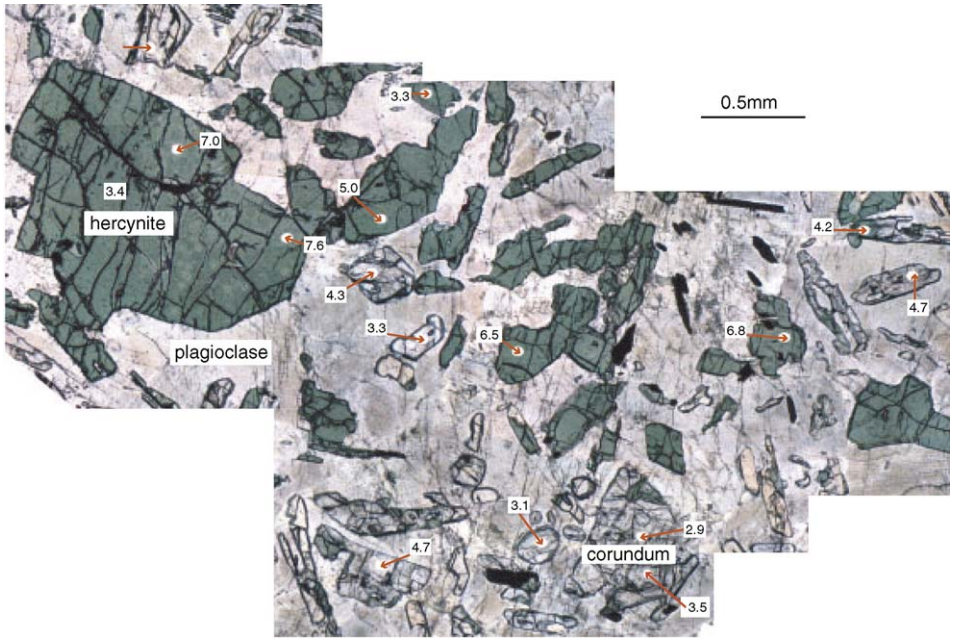

Fig. 5. Photomicrograph showing ion microprobe sites and distribution of $\delta^{18}O$ values in sample VB492–1005.0 from the south Eastern Deeps zone of the Viosey's Bay Intrusion. All $\delta^{18}O$ values are in per mil relative to VSMOW.

is not meaningful, but ranges obtained for distinct morphological types of hercynite obtained by ion probe are identical to those obtained by conventional analyses.

Over the course of the analytical sessions, instrumental mass fractionation for spinel 163728 varied between −1.8 and −2.3‰, and between +1.7 and −1.0‰ for laser ruby. The reproducibility of standards for individual sessions was ~1.0‰ (spinel 163728) and ~0.8‰ (laser ruby), which we adopt as the 1σ uncertainties for individual measurements.

5. Results

5.1. Ion microprobe $\delta^{18}O$ analyses of hercynite and corundum

Instrumental mass fractionation corrected results of ion microprobe $\delta^{18}O$ analyses of corundum from the different types of xenoliths are shown in Table 1, and are summarized in Fig. 2a, and those for hercynite are shown in Table 2 and are summarized in Fig. 2b. $\delta^{18}O$ values for corundum range between 1.9 and 6.1‰, and average 5.0‰. The range of observed $\delta^{18}O$ values of corundum in this study spans the mafic host rock and desilicated protolith environments of [16]. $\delta^{18}O$ values for the three types of hercynite range between 2.5 and 11.5‰. Acicular hercynite has $\delta^{18}O$ values that range between 2.5 and 7.6‰. Bulbous hercynite yields $\delta^{18}O$ values that range between 5.0 and 11.5‰. Granular hercynite yields $\delta^{18}O$ values that range between 6.7 and 10.4‰.

Figs. 3–6 show the sites of in situ ion microprobe analyses for oxygen isotopic compositions of hercynites and corundum from various xenoliths. Figs. 3 and 6 illustrate sections of light-cored xenoliths that contain composite grains of corundum and hercynite. In both sections a sharp replacement front separates hercynite from corundum. Three analyses of granular

Fig. 6. Photomicrograph showing ion microprobe sites and distribution of $\delta^{18}O$ values in sample VB523–762.0 from the Eastern Deeps zone of the Viosey's Bay Intrusion. All $\delta^{18}O$ values are in per mil relative to VSMOW.

hercynites shown in Fig. 3 yield $\delta^{18}O$ values of 6.7, 8.6, and 9.1‰. Acicular corundum in the same section has $\delta^{18}O$ values that range from 4.6 to 5.9‰. Two analyses of composite grains of corundum and hercynite yield $\delta^{18}O$ values of 4.9 and 5.2‰ for the corundum, and the associated hercynites have relatively higher $\delta^{18}O$ values of 6.5‰. Bulbous hercynite illustrated in Fig. 4 is characterized by $\delta^{18}O$ values that range from 6.0 to 11.5‰, and a single analysis of granular hercynite has a $\delta^{18}O$ value of 10.2‰. Acicular hercynite from the same section has $\delta^{18}O$ values that range from 2.5 to 5.9‰. Corundum has the lowest range of $\delta^{18}O$ values between 1.9 and 3.7‰.

Figs. 5 and 6 contain randomly distributed bulbous, acicular, and granular hercynites, as well as corundum and plagioclase. Both sections lack sharp replacement fronts that separate corundum from hercynite. Bulbous hercynites shown in Fig. 5 have $\delta^{18}O$ values that range from 5.0 to 7.6‰, and corundum has $\delta^{18}O$ values that range from 2.9 to 4.7‰. Bulbous and granular hercynites from the sample illustrated in Fig. 6 are characterized by $\delta^{18}O$ values that range from 7.5 to

Table 3
Oxygen isotopic values (conventional analyses) for pyroxene and garnet from country rocks and plagioclase from xenoliths

Drill core or sample #	Depth (m)	Type of sample	Rock type	Mineral	$\delta^{18}O$ (‰ VSMOW)
VB433	109	Regional	Tasiuyak Gneiss	Pyroxene	8.0
VB487	581.5	Aureole	Tasiuyak Gneiss	Pyroxene	8.3
VB192	293	Aureole	Tasiuyak Gneiss	Pyroxene	8.8
VB433	115	Regional	Tasiuyak Gneiss	Pyroxene	9.0
TG2	Outcrop	Regional	Tasiuyak Gneiss	Pyroxene	9.1
VB487	407.5	Aureole	Tasiuyak Gneiss	Pyroxene	9.3
VB433	109	Regional	Tasiuyak Gneiss	Pyroxene	9.3
TG3	Outcrop	Regional	Tasiuyak Gneiss	Pyroxene	9.4
VB487	407.5	Aureole	Tasiuyak Gneiss	Pyroxene	9.6
TG1	Outcrop	Regional	Tasiuyak Gneiss	Pyroxene	9.6
VB433	119.5	Aureole	Tasiuyak Gneiss	Pyroxene	10.1
S1	Outcrop	Regional	Nain Mafic Gneiss	Pyroxene	6.1
S1	Outcrop	Regional	Nain Mafic Gneiss	Pyroxene	6.3
VB192	252.7	Aureole	Enderbitic Gneiss	Pyroxene	5.7
VB264	104.2	Regional	Enderbitic Gneiss	Pyroxene	6.2
VB264	104.2	Regional	Enderbitic Gneiss	Pyroxene	6.9
VB192	243	Aureole	Enderbitic Gneiss	Pyroxene	7.5
VB192	293	Aureole	Tasiuyak Gneiss	Garnet	8.5
VB192	293	Aureole	Tasiuyak Gneiss	Garnet	8.8
VB487	407.5	Aureole	Tasiuyak Gneiss	Garnet	8.9
VB433	115	Regional	Tasiuyak Gneiss	Garnet	9.0
VB433	152	Aureole	Tasiuyak Gneiss	Garnet	9.1
TG2	Outcrop	Regional	Tasiuyak Gneiss	Garnet	9.1
VB487	581.5	Aureole	Tasiuyak Gneiss	Garnet	9.2
TG3	Outcrop	Regional	Tasiuyak Gneiss	Garnet	9.6
VB433	118	Aureole	Tasiuyak Gneiss	Garnet	9.8
VB487	361	Aureole	Tasiuyak Gneiss	Garnet	10.3
VB487	361	Aureole	Tasiuyak Gneiss	Garnet	10.1
TG1	Outcrop	Regional	Tasiuyak Gneiss	Garnet	10.0
VB433	119.5	Aureole	Tasiuyak Gneiss	Garnet	10.2
VB487	407.5	Aureole	Tasiuyak Gneiss	Garnet	10.4
VB433	152	Aureole	Tasiuyak Gneiss	Garnet	10.7
VB433	107	Regional	Tasiuyak Gneiss	Garnet	10.8
VB510	566	Xenolith		Plagioclase	8.1
VB510	566	Xenolith		Plagioclase	7.9
VB522	585	Xenolith		Plagioclase	9.5
VB522	585	Xenolith		Plagioclase	9.1
VB487	647	Xenolith		Plagioclase	10.4
VB492	1005	Xenolith		Plagioclase	7.1
VB523	762	Xenolith		Plagioclase	6.2

11.5‰, and 7.0 to10.4‰, respectively. In cases where corundum shares a grain boundary with hercynite the corundum consistently yields a relatively low $\delta^{18}O$ value compared to that of hercynite. Corundum shown in Fig. 6 has $\delta^{18}O$ values that range from 3.6 to 6.1‰.

5.2. $\delta^{18}O$ analyses of pyroxene, garnet, and plagioclase

Results of conventional $\delta^{18}O$ analyses of pyroxene and garnet from the country rocks are listed in Table 3. $\delta^{18}O$ values of pyroxene vary from 5.7 to 10.1‰. Pyroxene from the Tasiuyak paragneiss yields $\delta^{18}O$ values that range between 8.0 and 10.1‰, and pyroxene from the enderbitic and mafic orthogneisses has values that range between 5.7 and 7.5‰. Garnet from the Tasiuyak Gneiss is characterized by $\delta^{18}O$ values that range between 8.5 and 10.8‰. The average $\delta^{18}O$ value for garnet is 9.7‰. $\delta^{18}O$ values of plagioclase in the same xenoliths from which ion microprobe analyses were obtained range from 6.2 to 10.4‰ (Table 3).

6. Discussion

6.1. Pseudomorphic replacement of minerals in xenoliths and isovolumetric reactions

The composite grains of corundum and hercynite are interpreted as evidence for pseudomorphic replacement of corundum by hercynite. The close association of bulbous hercynite and garnet in the contact aureole, together with the fact that bulbous hercynite in the xenoliths defines the same textures as garnet, is interpreted as evidence that bulbous hercynite is a pseudomorph of garnet. This interpretation is augmented by the fact that bulbous hercynite is usually surrounded by granular and/or vermicular textured hercynite, defining a texture that resembles the symplectitic intergrowths in the Tasiuyak Gneiss which formed during the incipient stages of garnet breakdown in the contact aureole. The fact that granular hercynites exhibit the same grain shapes and textures as granular orthopyroxene in the protolith assemblage is interpreted as evidence for pseudomorphous replacement of pyroxene by hercynite.

Pseudomorphous hercynite, together with relict protolith textures such as crenulation cleavage and gneissic banding that are exhibited by the xenoliths in the Voisey's Bay Intrusion [1], imply that volume was conserved during mineral replacement reactions. The development of pseudomorphic textures requires that the rate of dissolution of the precursor mineral be similar to that of the simultaneous precipitation of the new mineral [17–19], thereby conserving volume. The following isovolumetric reactions are postulated to account for the dissolution of garnet, pyroxene and corundum and simultaneous precipitation of hercynite (although Mg is also a component of hercynite, for simplicity only Fe end-members are shown):

$$\overset{\text{Garnet}}{Fe_3Al_2Si_3O_{12(s)}} + 1.7\overset{\text{Melt(1)}}{Al_2O_{3(melt)}} \Rightarrow 2.7\overset{\text{Hercynite}}{FeAl_2O_{4(s)}} + 3\overset{\text{Melt}}{SiO_{2(melt)}} + 0.3FeO_{(melt)} \quad (1)$$

$$1.3\overset{\text{Hypersthene}}{FeSiO_{3(s)}} + \overset{\text{Melt(1)}}{Al_2O_{3(melt)}} \Rightarrow \overset{\text{Hercynite}}{FeAl_2O_{4(s)}} + 1.3\overset{\text{Melt}}{SiO_{2(melt)}} + 0.3FeO_{(melt)} \quad (2)$$

$$1.6\overset{\text{Corundum}}{Al_2O_{3(s)}} + \overset{\text{Melt(2)}}{FeO_{(melt)}} \Rightarrow \overset{\text{Hercynite}}{FeAl_2O_{4(s)}} + 0.6\overset{\text{Melt}}{Al_2O_{3(melt)}} \quad (3)$$

Reaction (1) is thought to have produced bulbous hercynite that is pseudomorphous after garnet. Isovolumetric replacement of garnet by hercynite via reaction (1) requires addition of Al and O, and releases SiO_2 and FeO to the melt (SiO_2/FeO = 10). Reaction (2) is thought to have produced granular hercynite that is pseudomorphous after pyroxene. Reaction (2) requires input of Al and O, and releases SiO_2 and FeO to the enclosing melt in the ratio of ~4:1. Both of these reactions are thought to have occurred during thermal equilibration of the xenoliths with surrounding magma, and synchronously with the initial formation of corundum via a reaction such as [1]:

$$2.67\overset{\text{Ca–plagioclase}}{(Na_{0.7}Ca_{0.3}Al_{1.3}Si_{2.7}O_8)_{(s)}} \Rightarrow \overset{\text{Corundum}}{0.835Al_2O_{3(s)}} + \overset{\text{Ca–rich plagioclase}}{(Na_{0.2}Ca_{0.8}Al_{1.8}Si_{2.2}O_8)_{(s)}} + \overset{\text{Melt}}{0.835Na_2O_{(m)}} + 5SiO_{2(m)} \quad (4)$$

In effect, a partial melt derived from a pelitic or quartzofeldspathic xenolith would have also contained Al_2O_3 providing a source of Al for reactions (1) and (2). The replacement of corundum by hercynite via reaction (3) requires addition of FeO and loss of Al and O to the melt. This reaction is thought to have produced acicular hercynite that is pseudomorphous after corundum. Fe and Al necessary to promote isovolumetric reactions could have been derived from the enclosing magma or from the breakdown of minerals like garnet, biotite, pyroxene and corundum. Reactions (1)–(3) illustrate potential feedback mechanisms that may have played a role in the generation of hercynite. Aluminum potentially derived from feldspar

dissolution may have driven reactions (1) and (2). Iron released in these reactions may have in turn reacted with corundum in melanosomes to produce hercynite. In the case of quartzofeldspathic xenoliths or xenoliths derived from leucosomes a local source of Fe and Mg is not available. In this case Fe and Mg must be derived from the surrounding mafic magma.

6.2. Evidence of oxygen isotopic disequilibrium

Both pelitic and quartzofeldspathic country rocks in the Voisey's Bay area are characterized by plagioclase $\delta^{18}O$ values in the range of 10 to 15‰. Reaction (4) leads to the production of a slightly ^{18}O-enriched siliceous melt (see fractionation factors in supplemental Table 1). Modeling using either batch or fractional expulsion of this melt shows that produced corundum should be characterized by $\delta^{18}O$ values no lower than ~6.5 to 7‰. The $\delta^{18}O$ values of corundum (Table 1, Fig. 2a) indicate that isotopic exchange with a low-^{18}O reservoir has occurred. Taking a representative $\delta^{18}O$ value of mantle-derived basaltic magma of ~5.5‰, both corundum and hercynite should be characterized by $\delta^{18}O$ values near 2.5‰ if oxygen isotopic equilibrium with the magma was attained. Assuming an initial $\delta^{18}O$ value of 7‰ for corundum, values of the fractional approach to equilibrium (f) with mafic magma at 1100 °C range from 0.1 to 0.9. Δ values for plagioclase–corundum range from 0.2 to 6.1‰, and confirm that oxygen isotopic equilibrium was not attained during retrograde cooling.

Assuming that the Al_2O_3 component of reactions (1) and (2) was derived from feldspar, modeling of the replacement of a 10‰ garnet or pyroxene indicates that hercynite produced via these reactions should have been characterized by equilibrium $\delta^{18}O$ values of 7.6 to 8.7‰. More elevated $\delta^{18}O$ values that are found in several granular and bulbous hercynite grains must be inherited from protolith garnet or pyroxene, possibly with a contribution from the high-^{18}O partial melt produced in the feldspar–corundum conversion. However, the variability in hercynite $\delta^{18}O$ values indicates that hercynite did not uniformly equilibrate with either partial melt derived from feldspar breakdown or with enclosing basaltic magma (or crystal mush).

The replacement of acicular corundum by hercynite was initiated at the margins of xenoliths. The relatively high-^{18}O character of the hercynite presents an intriguing situation in terms of the paragenesis of ^{18}O exchange. Pseudomorphic replacement of corundum by hercynite must have involved ^{18}O-rich material derived from the xenoliths. Mixing between the expelled ^{18}O-rich partial melt derived from the pelitic and quartzofeldspathic xenoliths and mafic magma at the margins of the xenoliths is thought to have produced hybrid melt with elevated, and locally variable, $\delta^{18}O$ values. However, the low $\delta^{18}O$ values of corundum in cores of xenoliths strongly suggest that ^{18}O exchange with uncontaminated magma occurred prior to the development of the hercynite replacement front. Oxygen isotopic exchange with mafic magma appears to have occurred synchronously with the expulsion of siliceous melt from the xenoliths. The advance of the hercynite replacement front, driven by chemical potential gradients, followed the expulsion of partial melt from the xenoliths and initial ^{18}O exchange with corundum.

Mariga et al. [1] have described the crystallization of a band of plagioclase followed by a band of biotite around most xenoliths at Voisey's Bay. Formation of the bands was linked to the development of boundary layers enriched in Si, Na and K that were derived from the xenoliths. Only a fraction of the ^{18}O-rich partial melt expelled from the xenoliths is accounted for in the bands that surround the xenoliths. Biotite is characterized by isotopically "normal" oxygen and hydrogen, suggestive of exchange with 5 to 6‰ mafic magma at the margins of xenoliths. The igneous matrix material reveals no evidence for the high-^{18}O melt lost from the xenoliths, and removal within magma which passed through the conduit system is thought to have occurred.

The formation of plagioclase and biotite bands appears to have strongly affected both chemical and isotopic characteristics of the xenoliths. Although biotite records oxygen isotopic equilibration with mafic magma, the bands appear to have armored the xenoliths and reduced isotopic communication with surrounding melt. Iron and magnesium required for the replacement of corundum by hercynite were primarily derived from the magma which produced the plagioclase band. The sharp corundum–hercynite replacement front is coupled to the depletion of Fe and Mg in the plagioclase band. Although a record of non-equilibrium oxygen isotopic exchange with surrounding melt is preserved due to the formation of plagioclase and biotite bands, it is nonetheless surprising that at the temperature attained by the xenoliths, internal oxygen isotopic equilibration between hercynite, corundum and plagioclase was not established interiorly to the biotite band.

6.3. Potential causes of oxygen isotopic disequilibrium

Oxygen isotopic disequilibrium among minerals in xenoliths within the Voisey's Bay Intrusion may have arisen during partial melting that gave rise to corundum and hercynite as products of the decomposition of plagioclase

and garnet/pyroxene, respectively. The rapid withdrawal of partial melt from the xenoliths may have prevented oxygen isotopic equilibration [20–22]. The initial replacement of corundum by hercynite may have involved the diffusive transport of FeO and MgO from contaminated, ^{18}O-rich mafic magma at margins of inclusions [2]. Gradients of ^{18}O between unreplaced corundum and hercynite would be expected as a result of the reaction between corundum and transported FeO and MgO.

According to the fractionation factors of [23,24; supplemental Table 1], corundum and hercynite would be characterized by nearly identical δ^{18}O values, and hence diffusive transport of oxygen would have been expected to erase δ^{18}O variations. As an example, an acicular grain of hercynite and corundum with different oxygen isotopic signatures (e.g. Figs. 3, 4 and 6) may be viewed as a diffusion couple. A solution to the diffusion equation for this geometry is [25]:

$$C(x,t) = (C_1 + C_2)/2 - (C_1 - C_2)/2(\mathrm{erf}(x/(2(Dt)^{1/2}))) \quad (5)$$

where, x is distance, erf is the error function, D is oxygen diffusivity, C_1 is the oxygen isotopic composition of hercynite, and C_2 is the oxygen isotopic composition of corundum. Values of D for oxygen in corundum are known only for temperatures above 1220 °C [26], but are in excess of 10^{-8} cm^2/s. Although D values for oxygen diffusion in Fe-rich hercynite are unknown, those for Mg–Al oxide and magnetite are greater than 10^{-9} cm^2/s. Even assuming D values as low as 10^{-10} cm^2/s at temperatures between 700 and 900 °C, Eq. (5) predicts that for a 2 mm long acicular grain, nearly complete isotopic homogenization could have been attained within less than ~1000 years. The length of time that the magmatic system at Voisey's Bay was operative is difficult to estimate. Geochronologic studies [27,28] suggest that intrusive activity associated with the Nain Plutonic Suite lasted, at least intermittently, for approximately 30 Ma. The Kiglapait and Newark Island Intrusions (Fig. 1) have been dated at 1306 and 1305 Ma, respectively, whereas the Mushuau Intrusion located just to the north of the Voisey's Bay Intrusion crystallized between 1313 and 1317 Ma [29–31]. The Voisey's Bay Intrusion has been dated at 1332 +/− 2 Ma and is the oldest troctolitic intrusion currently known in the Nain Plutonic Suite [27]. Although magma flow in any particular conduit may have been episodic or restricted to a relatively short time interval, it is unlikely that temperatures in the surrounding magma or within the xenoliths declined so rapidly as to prevent diffusive transport of oxygen in the acicular grains of corundum and hercynite. The fact that oxygen isotopic homogenization is not observed suggests either that estimates of corundum–hercynite oxygen isotopic fractionation factors are in error, or that chemical reaction was required to produce the oxygen isotopic distributions in the xenoliths at Voisey's Bay. Even though the corundum–hercynite fractionation factors are based on theoretical computations [16] and must be viewed with caution, the variability in Δ (hercynite–corundum) values indicate that isotopic equilibrium has not been attained, and that oxygen diffusion was not an effective mechanism for isotopic exchange.

7. Conclusions

The elevated δ^{18}O values of hercynite that has replaced garnet and/or pyroxene in xenoliths from the Voisey's Bay Intrusion must largely represent the inheritance of ^{18}O-

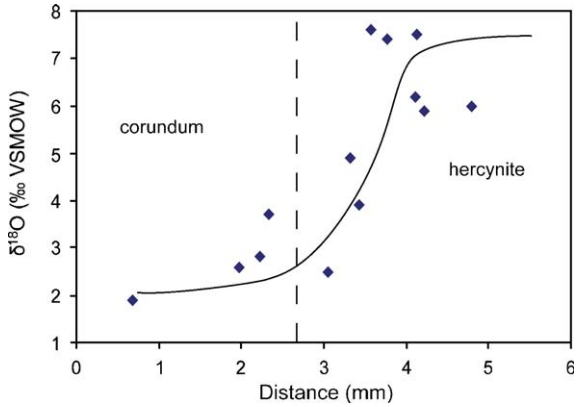

Fig. 7. δ^{18}O profile of a two millimeter wide traverse across the corundum–hercynite rim of sample VB510–566 shown in Fig. 4. Isotopic values were projected within the two millimeter width radially along curves parallel to the corundum–hercynite contact to a traverse line running from the lower left to the upper right in Fig. 4.

enriched oxygen from protolith minerals. Ion microprobe analyses confirm that this type of hercynite did not equilibrate with either partial melts derived from the xenoliths or with mafic magma in which the xenoliths were immersed. Iron and magnesium required for the replacement of corundum by hercynite must have come from the magma, in contrast to hercynite derived from garnet or pyroxene. However, the $\delta^{18}O$ values of hercynite which replaces corundum are also spatially variable, and strongly indicative of the lack of oxygen isotopic equilibrium on the sub-millimeter scale. The crystallization of plagioclase and biotite bands around xenoliths is thought to have prevented isotopic communication between xenoliths and magma, and to be responsible for the preservation of non-equilibrium oxygen isotopic distributions.

Fig. 7 illustrates that an oxygen isotopic profile across the hercynite–corundum replacement front in a light-cored xenoliths is nearly as sharp as the chemical front, and that a potential diffusive exchange zone is limited to less than 1.5 mm. In individual grains where corundum and hercynite are in direct contact, the oxygen isotopic profile approximates a step function. Neither the initial replacement of corundum by hercynite, nor retrograde cooling has lead to the attainment of oxygen isotopic equilibration between hercynite and corundum. Modeling of diffusive oxygen transport in corundum suggests that isotopic homogenization (in this case equilibrium between hercynite and corundum) could have been attained in less than ~1000 years at temperatures between ~700 and 1000 °C. Even though magma flow in the conduit system at Voisey's Bay system may have been episodic in nature, it is unlikely that temperatures of the surrounding magma were not maintained for sufficient intervals of time to permit diffusive oxygen isotopic exchange. In the xenoliths within the Voisey's Bay Intrusion the cessation of corundum replacement by hercynite coincided with the depletion of Fe and Mg within the surrounding band of plagioclase crystallization and with terminal oxygen isotopic exchange. Isotopic gradients and homogenization across corundum–hercynite grain boundaries on a scale of tens to hundreds of microns are not observed, and suggest that the primary mechanism of oxygen isotopic exchange in the system must be related to reaction and recrystallization.

Acknowledgements

This work was supported by the National Science Foundation grant EAR-0086538 to E.M.R. We acknowledge constructive criticisms and reviews by James Brophy, Robert Wintsch, Erika Elswick, and two EPSL reviewers. Staff and geologists of the Voisey's Bay Nickel Company, particularly Dan Lee and Dawn Evans-Lamswood, are thanked for granting access to samples and for constructive discussions. Steve Studley, Jon Fong, Peter Sauer and Arndt Schimmelmann of the Indiana University Stable Isotope Research Facility are thanked for technical assistance.

Appendix A. Supplementary data

Supplementary data associated with this article can be found, in the online version, at doi:10.1016/j.epsl.2006.05.031.

References

[1] J. Mariga, E.M. Ripley, C. Li, Petrogenetic evolution of xenoliths at the Voisey's Bay Ni–Cu–Co deposit, Labrador, Canada: I Mine ralogy, reactions, partial-melting, and mechanisms of mass transfer, Geochem., Geophys., Geosys. 7 (2006) Q05013, doi:10.1029/2005GC001184.

[2] J. Mariga, E.M. Ripley, C. Li, Oxygen isotopic studies of the interaction between xenoliths and mafic magma, Voisey's Bay Intrusion, Labrador, Canada, Geochim. et Cosmochim. Acta (in press).

[3] C.R.M. McFarlane, W.D. Carlson, J.N. Connelly, Prograde, peak, and retrograde *P–T* paths from aluminum in orthopyroxene: high-temperature contact metamorphism in the aureole of the Makhavinekh Lake Pluton, Nain Plutonic Suite, Labrador, J. Metamorph. Geol. 21 (2003) 405–423.

[4] D. Lee, Geothermobarometry and Petrologic History of a Contact Metamorphosed Section of the Tasiuyak Gneiss, West of Nain, Labrador, Bachelor of Science (Honors), Memorial University of Newfoundland, St. John's NF, 1987.

[5] R.J. Wardle, Nain Churchill province cross-section, Nachvak Fiord, northern Labrador: Newfoundland Department of Mines and Energy, Mineral Development Division, Curr. Res. Report. 83-1 (1983) 68–90.

[6] R.J. Wardle, A.B. Ryan, G.A.G. Nunn, F.C. Mengel, Labrador segment of the trans-Hudson orogen: crustal development through oblique convergence and collision, in: J.F. Lewry, M.R. Stauffer (Eds.), The Trans-Hudson Orogen of North America: Lithotectonic Correlations and Evolution, Geol. Assoc. Canada Special Paper, vol. 37, 1990, pp. 353–370.

[7] R.J. Wardle, A.B. Ryan, S. Philippe, U. Schärer, Proterozoic crustal development, Goose Bay region, Grenville Province, Labrador, Canada, in: C.F. Gower, T. Rivers, B. Ryan (Eds.), Mid-Proterozic Laurentia-Baltica, Geol. Assoc. Canada, Special Paper, vol. 38, 1990, pp. 197–214.

[8] B. Ryan, The Nain–Churchill boundary and the Nain Plutonic Suite: a regional perspective on the geologic setting of the Voisey's Bay Ni–Cu–Co deposit, Econ. Geol. 95 (2000) 703–724.

[9] B. Ryan, R.J. Wardle, C. Gower, G.G. Nunn, Nickel–copper sulfide mineralization in Labrador: the Voisey's Bay discovery and its exploration implications, Current Research, Newfoundland Department of Natural Resources, Geol. Surv. Rep. 95-1 (1995) 177–204.

[10] J. Berg, J. Docka, Geothermometry in the Kiglapait contact aureole, Labrador, Am. J. Sci. 283 (1983) 414–434.

[11] R.F. Emslie, M.A. Hamilton, R.J. Thermal, Petrogenesis of mid-Proterozoic anorthosite–mangerite–chanockite–granite (AMCG) complex: isotopic and chemical evidence from the Nain Plutonic Suite, J. Geol. 102 (1994) 539–558.
[12] A.J. Naldrett, H. Keats, K. Spakes, R. Moore, Geology of the Voisey's Bay Ni–Cu–Co deposit, Labrador, Canada, Explor. Min. Geol. 5 (1996) 169–179.
[13] A.J. Naldrett, World class Ni–Cu–PGE deposits: key factors in their genesis, Miner. Depos. 34 (1999) 227–240.
[14] R.N. Clayton, T.K. Mayeda, The use of bromine pentaflouride in the extraction of oxygen from oxides and silicates for isotopic analysis, Geochim. Cosmochim. Acta 27 (1963) 43–52.
[15] S.S. Russell, G.J. MacPherson, L.A. Leshin, K.D. McKeegan, ^{16}O enrichment in aluminum-rich chondrules from ordinary chondrites, Earth Planet. Sci. Lett. 184 (2000) 57–74.
[16] G. Giuliani, A.E. Fallick, V. Garnier, C. France-Lanord, D. Ohnenstetter, D. Schwarz, Oxygen isotope composition as a tracer for the origins of rubies and sapphires, Geology 33 (2005) 249–252.
[17] D.S. Korzhinskii, Theory of Metasomatic Zoning (translated by Jean Agrell), Oxford Clarendon Press, Oxford, 1970, 162 pp.
[18] A. Hoffman, Chromatographic theory of infiltration metasomatism and its application to feldspars, Am. J. Sci. 272 (1972) 69–90.
[19] D. Nahon, E. Merino, Pseudomorphic replacement in tropical weathering: evidence, geochemical consequences, and kinetic–rheological origin, Am. J. Sci. 297 (1999) 393–417.
[20] G.R. Davies, S. Tommasini, Isotopic disequilibrium during rapid crustal anatexis: implications for petrogenetic studies of magmatic processes, Chem. Geol. 162 (2000) 169–191.
[21] K.M. Knesel, J.P. Davidson, Isotopic disequilibrium during melting of granite and implications for crustal contamination of magmas, Geology 24 (1996) 243–246.
[22] L. Barbero, C. Villaseca, G. Rogers, P.E. Brown, Geochemical and isotopic disequilibrium in crustal melting: an insight from the anatectic granitoids from Toledo, Spain, J. Geophys. Res. 100 (1995) 15745–15765.
[23] Y.F. Zheng, Calculation of oxygen isotope fractionation in metal oxides, Geochim. Cosmochim. Acta 55 (1991) 2299–2307.
[24] Z.F. Zhao, Y.F. Zheng, Calculation of oxygen isotope fractionation in magmatic rocks, Chem., Geol. 193 (2003) 59–80.
[25] J. Crank, The Mathematics of Diffusion, 2nd ed. Oxford University Press, London, 1995, 414 pp.
[26] D.R. Cole, S. Chakraborty, Rates and mechanisms of isotopic exchange, in: J.W. Valley, D.R. Cole (Eds.), Stable Isotope Geochemistry, Rev. Mineral. Geochem., vol. 43, 2001, pp. 83–223.
[27] Y. Amelin, C. Li, A.J. Naldrett, Geochronology of the Voisey's Bay intrusion, Labrador, Canada, by precise U–Pb dating of coexisting baddeleyite, zircon, and apatite, Lithos 47 (1999) 33–51.
[28] Y. Amelin, C. Li, O. Valayev, A.J. Naldrett, Nd–Pb–Sr isotope systematics of crustal assimilation in the Voisey's Bay and Mushuau intrusions, Labrador, Canada, Econ. Geol. 95 (2000) 815–830.
[29] S.A. Morse, Kiglapait mineralogy III: olivine compositions and Rayleigh fractionation model, J. Petrol. 37 (1996) 1037–1061.
[30] K.R. Simmons, R.A. Weibe, G.A. Snyder, E.C. Simmons, U–Pb zircon age for the Newark Island layered intrusion, Nain Anorthosite Complex, Geol. Soc. Am. Abs. w. Prog., vol. 18, 1986, p. 751.
[31] C. Li, P.C. Lightfoot, Y. Amelin, A.J. Naldrett, Contrasting petrological and geochemical relationships in the Voisey's Bay and Mushuau Intrusions, Labrador, Canada: implications for ore genesis, Econ. Geol. 95 (2000) 771–799.